Mathematical Statistician and Engineering Applications
ISSN: 2094-0343
2326-9865

2D and 3D Shapes of Elliptical Galaxies NGC 1199, 1395 and NGC 1549

Arun Kumar Diwakar [1], Aloke Verma [2], Avinash Singh [2], Tripti Richhariya [2], Ekta Chandrawanshi[2] & Laxmikant Chaware [3]

[1]Department of Physics, Govt. MRG College, Kondagaon (C.G.) India 494226

[2]Department of Physics, Kalinga University, Naya Raipur (CG) India 492101

[3]Centre for Basic Sciences, Pt. Ravishankar Shukla University, Raipur (CG) India 492010

Corresponding Author Email ID: aloke.verma@kalingauniversity.ac.in; diw.arun@gmail.com

Article Info
Page Number: 29-37
Publication Issue:
Vol. 72 No. 1 (2023)

Article History
Article Received: *15 October 2022*
Revised: *24 November 2022*
Accepted: *18 December 2022*

Abstract

Photometric data from the literature is combined with triaxial mass models to derive 2D and 3D shapes of the light distribution of elliptical galaxies NGC 1199; 1395 and 1549. The inferred shape variation in given by a Bayesian probability distribution, assuming a uniform prior. The likelihood of obtaining the data is calculated by using ensemble of triaxial models. We apply the method to infer the shape variation of a galaxy, using the ellipticities and the difference in the position angles at two suitably chosen points from the profiles of the photometric data. Best constrained shape parameters are found to be the short to long axial ratios at small and large radii, and the absolute values of the triaxiality difference between these radii.

Keywords: Galaxy - Photometric, Galaxy - Intrinsic Shape, NGC 1199; 1395 and 1549.

1. Introduction

Intrinsic shapes of the individual elliptical galaxies have been investigated by Binney (1985), Tenjes et. al. (1993), Statler (1994a; b), Bak & Statler (2000), Statler (2001) and Statler, Emsellem, Peletier and Bacon (2004). These authors have used the kinematical data and the photometric data, and have used the triaxial models with the density distribution $\rho(m^2)$, where $m^2 = x^2 + \frac{y^2}{p^2} + \frac{z^2}{q^2}$ with axial ratios p and q. Here, (x, y, z) are the usual Cartesian co-ordinates, oriented such that $x-$ axis ($z-$ axis) lies along the longest (the shortest) axis of the model. It was shown analytically that the projected density of such a distribution $\rho(m^2)$ with constant $(p; q)$ is stratified on similar and co-aligned ellipses (Satrk 1977, Binney 1985). Statler (1994a, b, hereafter S 94a, S 94b) uses (apart from the kinematical data) a constant value of ellipticity, which is an average over a suitably chosen range of radial distance, for the shape estimates. The shape estimates are robust, and are described by a pair of the shape parameters, namely the short to long axial ratio cL of the light distribution and the triaxiality TM of the mass distribution. A complementary problem was attempted by Chakraborty, Singh and Gaffar (2008) and Chakraborty, Diwakar and Pandey (2011, hereafter C11) wherein variation in the intrinsic shapes of elliptical galaxies was investigated by using triaxial models which exhibit ellipticity variation and position angles twist. These models are fixed by assigning the values

of axial ratios (p_0, q_0) and (p_∞, q_∞) at small and at large radii, respectively. These axial ratios are related to triaxialities T_0 and T_∞, respectively, at small and large radii. The intrinsic shape is described by parameters $(q_0, T_0, q_\infty, T_\infty)$. It is found that while triaxialities T_0 and T_∞ are not constrained, flattening (q_0, q_∞) are well constrained. It is found that the best constrained shape parameters are (q_0, q_∞) and the absolute value of the triaxiality difference $|T_d|$, defined as $|T_d| = |T_\infty - T_0|$. C11 have estimated the shapes of 3 elliptical galaxies which are comparatively very flat.

2. Shapes Parameters

It is necessary to find the parameters which are best constrained. These parameters will be used to describe intrinsic shape, and will be called as shape parameters. These are not known, a priori and suitable numerical investigation are needed for this. One method is to find correlation between the projected parameters when a model with a chosen set of intrinsic parameters is projected in all viewing angles. This method is adopted in Statler and Fry (1994). Thakur and Chakraborty (2001) also find such correlation plots. We adopt a more direct method. The intrinsic parameters of our models are $(p_0, q_0, p_\infty, q_\infty)$. We take any two of them, calculated MPD by summing over the remaining two parameters, to find those parameters which are best constrained. these parameters can be used as shape parameter.

3. Shapes Estimations

First, we take on shape parameters (q_0, q_∞). We consider a model with a chosen intrinsic parameter (q_0, q_∞). For each choice of (q_0, q_∞), we choose number of the values of (T_0, T_∞) and project the resultant model $(\gamma = 1{:}5)$ is chosen in some viewing angles (θ', ϕ'). We calculate the project properties of ellipticity and position angles by using appropriate analytical formula as mentioned in previous section. We calculate the likelihood by formula. We choose the error in ellipticities at R_{in} and R_{out} as $0{:}01$, which is typical error in the observation and chosen an error of 1σ in position angle, again as a typical error in observation. This gives the error in position angles differences as $\sqrt{2}$.

We multiply the likelihood by prior density, which we take as 1 (flat prior) and integrate over the uninteresting parameters and sum over (un-weighted sum) over choices of (T_0, T_∞). These gives MPD for each choice of (q_0, q_∞). The results of MPD as a function of shape parameters (q_0, q_∞) is presented in plot $1, 2$. We Choose the 48×48 values of (q_0, q_∞) spans the entire parameter space of $(q_0, q_\infty)$and for each (q_0, q_∞), we take 6×6 values of $(T_0, T_\infty)$the covering range of (T_0, T_∞). Plots demonstrate that (q_0, q_∞) are constrained. HPD area cover a small part in the parameters space of parameters (q_0, q_∞).

4. Observational Data

The morphological classification of NGC 1199; 1395 and 1549 are $E_3/E_2, E_2/E_3$ and E_0 respectively, from RC2 (de Vaucouleurs et. al., 1977) catalogue. The apparent flattening of a elliptical galaxy depends on the intrinsic flattening and the orientation. Further, the marginal posterior density (MPD) of the Bayesian estimate gives the most probable intrinsic shape which reproduces the data over a greatest variety of the orientations. To gain some insight into the

possible values of the intrinsic shape, which will be obtained by Bayesian method, we perform the following numerical experiments. The observational data used in the models of these galaxies are presented in table 1.

Table 1. Observational data of the galaxies.

Galaxy	$\mathbf{R_e}$	$\mathbf{R_{in}}$	$\mathbf{R_{out}}$	$\boldsymbol{\varepsilon_{in}}$	$\boldsymbol{\varepsilon_{out}}$	$\boldsymbol{\theta_d}$
NGC1199	29.0	12.63	39.53	0.26	0.20	2.0
NGC1395	45.0	12.63	39.53	0.16	0.20	7.0
NGC1549	48.0	12.59	39.53	0.15	0.13	22.0

5. 2D and 3D shapes of NGC 1199

The observe data of NGC 1199, is taken from R-band surface photometry of Franx et al. (1989). The ellipticity ε increases monotonically from 0.26 at $R_{in} = 12.63$ arcsec to 0.20 at $R_{out} = 39.53$ arcsec. In this range, the position angle decreases by $2.0°$. We consider the uncertainty in the ellipticity as 0.20 and in the position angle is $1.0°$, both at R_{in} and at R_{out}. These are the typical errors in observations. The effective radius of the galaxy is 29.0 arcsec. We use the ensemble of models, as described in Chakraborty and Diwakar (2011), with $\beta = 5.0, 1.0, 0.2$ and $\alpha = 0.0, 2.5, 5.0$. Integrating the marginal posterior density over all possible values of (T_0, T_∞), and taking unweighted sum over all these models, we obtained shape estimate $\mathcal{P}$ as a function of (q_0, q_∞).

Table 2. Statistical summary of the 2D shape of the NGC 1199 using the limits 0.4 to 1.0, both for q_0 and q_∞.

Model	$< \mathbf{q_{0p}} >$	$< \mathbf{q_{\infty p}} >$	$< \mathbf{q_0} >$	$< \mathbf{q_\infty} >$	**HPD**
$\beta = 0.2$	0.61	0.79	0.58	0.74	10.02
$\beta = 1.0$	0.68	0.81	0.59	0.87	10.59
$\beta = 5.0$	0.69	0.96	0.60	0.87	12.93
$\alpha = 0.0$	0.70	0.93	0.61	0.87	7.50
$\alpha = 2.5$	0.70	0.93	0.61	0.87	7.50
$\alpha = 5.0$	0.76	0.95	0.66	0.88	5.07
$\sum$ of all Model	**0.76**	**0.95**	**0.66**	**0.88**	**5.07**

Figure 1 presents the 2D shape estimate (q_0, q_∞) of NGC 1199, wherein we have allowed the limits $0{:}\,4$ to $1{:}\,0$ both for q_0 and q_∞. The probability of the shape plotted in dark grey shade: darker is the shade, higher is the probability. The white contour encloses the region of 68%

highest posterior density, which may be interpreted as 1σ error bar. We find that the 1σ region is very narrow which should be the consequence of the limits of q_0 and q_∞ taken. Although, it is the plot of $\mathcal{P}$ as a function of shape parameters, which constitute the Bayesian estimate of the shape, some statistical summary of the shape is very convenient for its description. The expectation values $< q_0 >$, $< q_\infty >$ and location of the peak values $< q_{0p} >$, $< q_{\infty p} >$ are such quantities. Table 2 provides such a summary. The expectation values of the flattening at small and at large radii are $< q_0 > = 0.66$ and $< q_\infty >= 0.88$, respectively. Table 2 gives a summary of 2D shape as presented in figure 1. Figure 2 and table 3 show the 3-dimensional intrinsic shape of NGC 1199 as a function of (q_0, q_∞) and $|T_d|$. We cut a total of 16 sections, each perpendicular to$|T_d|$ axis, and arrange these sections in a form of a two-dimensional array. The value of $|T_d|$is constant in each section, and is shown in the plot. We find

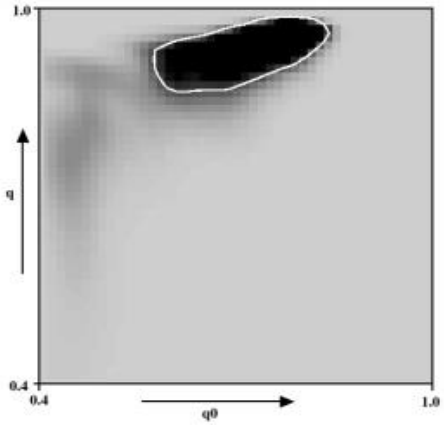

Figure 1. Plot of MPD ($\mathcal{P}$) as a function of $q_0, q_\infty (= q)$, summed over various values of (T_0, T_∞) for NGC 1199 using the limits 0.4 to 1.0, both for q_0 and q_∞.

Table 3. Statistical summary of the 3D shape of the NGC 1199 using the limits 0.4 to 1.0, both for q_0 and q_∞.

Model	$< q_{0p} >$	$< q_{\infty p} >$	T_0	$< q_0 >$	$< q_\infty >$	T_∞	**HPD**
$\beta = 0.2$	0.61	0.79	0.093	0.58	0.70	0.31	12.62
$\beta = 1.0$	0.67	0.79	0.031	0.59	0.75	0.27	9.31
$\beta = 5.0$	0.67	0.97	0.031	0.59	0.83	0.32	15.06
$\alpha = 0.0$	0.67	0.85	0.093	0.55	0.79	0.36	11.31
$\alpha = 2.5$	0.61	0.91	0.021	0.60	0.86	0.36	5.5
$\alpha = 5.0$	0.55	0.91	0.031	0.62	0.86	0.35	5.06

∑ of all Model	**0.61**	**0.91**	**0.093**	**0.59**	**0.80**	**0.34**	**14.43**

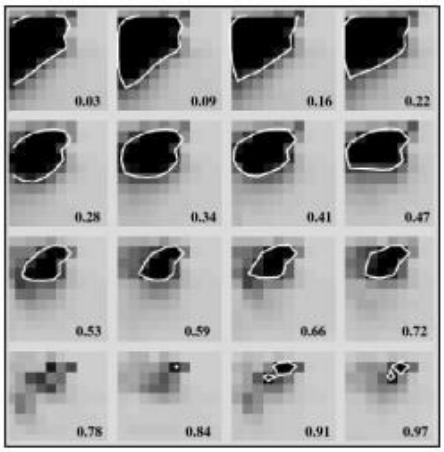

Figure 2. Three-dimensional plot of the unweighted sum of ($\mathcal{P}$) as a function of $q_0, q_\infty, |T_d|$, for NGC 1199.

The sum is taken over the M^2 models with $\beta = 0.2, 1.0, 5.0$ and the fgh models $\alpha = 0.02, 2.5, 5.0$ Values of $|T_d|$ are constant in each section. In each section, q_0 goes from the left to right hand side from 0.4 to 1.0, and q_∞ runs between the same values from the bottom to the top. that the 1σ region occupies larger area in the sections with smaller values of $|T_d|$. Further, in each section of constant $|T_d|$, 1 region occupies a small area of (q_0, q_∞) plane. We find that higher P is concentrated in sections with $|T_d|$ between 0.28 to 0.47. The expectation value of $< |T_d| >= 0.34$

Table 4. Statistical summary of the 2D shape of the NGC 1395 using the limits 0.4 to 1.0, both for q_0 and q_1.

Model	$< q_{0p} >$	$< q_{\infty p} >$	$< q_0 >$	$< q_\infty >$	**HPD**
$\beta = 0.2$	0.89	0.79	0.81	0.67	17.23
$\beta = 1.0$	0.84	0.74	0.73	0.69	19.53
$\beta = 5.0$	0.83	0.68	0.72	0.67	24.04
$\alpha = 0.0$	0.61	0.41	0.54	0.56	14.40
$\alpha = 2.5$	0.61	0.75	0.58	0.67	16.23
$\alpha = 5.0$	0.61	0.84	0.60	0.71	13.97
∑ of all Model	**0.68**	**0.84**	**0.60**	**0.71**	**14.23**

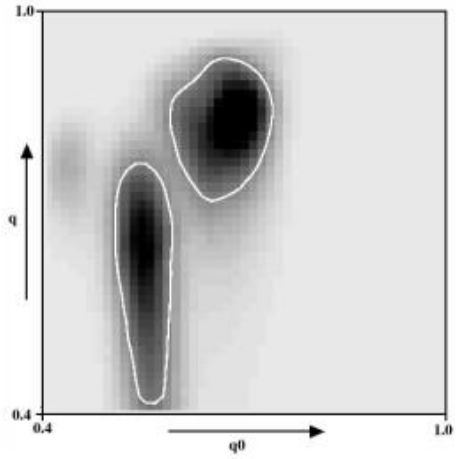

Figure 3. Same as Figure 1, for NGC 1395.

Table 5. Statistical summary of the 3D shape of the NGC 1395 using the limits 0:4 to 1:0, both for q0 and q1.

Model	$< q_{0p} >$	$< q_{\infty p} >$	T_0	$< q_0 >$	$< q_\infty >$	T_∞	**HPD**
$\beta = 0.2$	0.97	0.49	0.34	0.72	0.55	0.45	12.93
$\beta = 1.0$	0.67	0.49	0.21	0.70	0.56	0.40	11.06
$\beta = 5.0$	0.73	0.49	0.84	0.70	0.52	0.77	1.81
$\alpha = 0.0$	0.61	0.43	0.40	0.57	0.56	0.47	7.0
$\alpha = 2.5$	0.61	0.79	0.40	0.59	0.65	0.46	8.31
$\alpha = 5.0$	0.67	0.85	0.34	0.63	0.73	0.45	6.87
$\sum$ of all Model	**0.73**	**0.49**	**0.90**	**0.66**	**0.56**	**0.55**	**18.43**

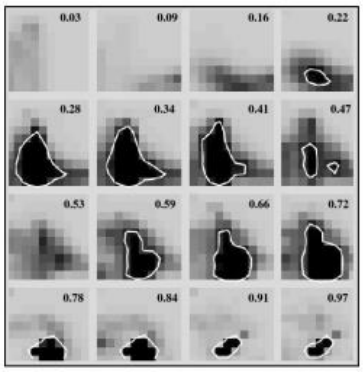

Figure 4. Same as Figure 2, for NGC 1395.

Table 6. Statistical summary of the 2D shape of the NGC 1549 using the limits 0.4 to 1.0, both for q_0 and q_∞.

Model	$< q_{0p} >$	$< q_{\infty p} >$	$< q_0 >$	$< q_\infty >$	**HPD**
$\beta = 0.2$	0.82	0.86	0.73	0.81	14.58
$\beta = 1.0$	0.81	0.89	0.69	0.87	15.40
$\beta = 5.0$	0.81	0.98	0.71	0.84	18.75
$\alpha = 0.0$	0.40	0.79	0.42	0.75	1.6
$\alpha = 2.5$	0.50	0.93	0.52	0.94	0.6
$\alpha = 5.0$	0.59	0.95	0.60	0.95	0.65
$\sum$ of all Model	**0.51**	**0.94**	**0.61**	**0.84**	**14.58**

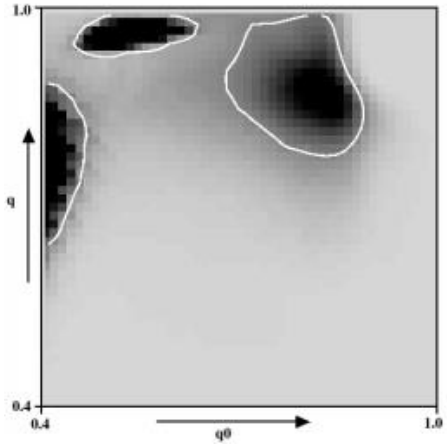

Figure 5. Same as Figure 1, for NGC 1549.

Table 7. Statistical summary of the 3D shape of the NGC 1549 using the limits 0.4 to 1.0, both for q_0 and q_∞.

Model	$< q_{0p} >$	$< q_{\infty p} >$	T_0	$< q_0 >$	$< q_\infty >$	T_∞	**HPD**
$\beta = 0.2$	0.55	0.73	0.78	0.54	0.74	0.77	1.5
$\beta = 1.0$	0.67	0.67	0.71	0.66	0.66	0.71	2.12
$\beta = 5.0$	0.73	0.49	0.84	0.70	0.52	0.77	1.81
$\alpha = 0.0$	0.43	0.73	0.84	0.43	0.68	0.82	0.31

$\alpha = 2.5$	0.43	0.91	0.84	0.44	0.92	0.78	0.25
$\alpha = 5.0$	0.61	0.97	0.71	0.59	0.95	0.67	0.37
$\sum$ of all Model	**0.43**	**0.91**	**0.84**	**0.56**	**0.74**	**0.75**	**4.18**

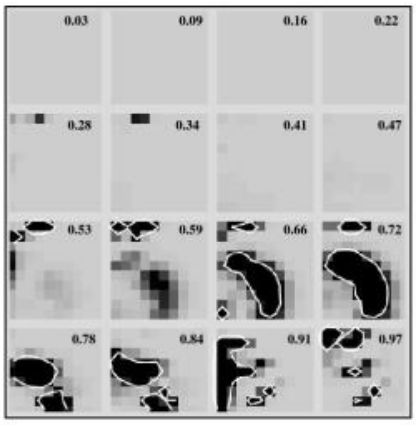

Figure 6. Same as Figure 2, for NGC 1549.

6. Conclusion

Table 8 gives a summary of intrinsic shapes of the elliptical galaxies as presented in figures 1, 3 and 5. The expectation values $< q_0 >, < q_\infty >$ and location of the peak values $< q_{0p} >, < q_{\infty p} >$ are such quantities. The expectation values of the flattening at small and at large radii are $< q_0 >$ and $< q_\infty >$, respectively.

Table 8. Statistical summary of the 2D shape of the NGC 1549 using the limits 0.4 to 1.0, both for q_0 and q_∞.

Galaxy	$< q_{0p} >$	$< q_{\infty p} >$	$< q_0 >$	$< q_\infty >$	**HPD**
NGC 1199	0.76	0.95	0.66	0.88	5.16
NGC 1395	0.68	0.84	0.60	0.71	14.23
NGC 1549	0.51	0.94	0.61	0.84	14.58

Table 9 show the summary of the 3D shapes of the elliptical galaxies, NGC 1199; 1395 and NGC 1549 as a function of q_0, q_∞ and $|T_d|$, presented in figures in previous section.

Galaxy	$< q_{0p} >$	$< q_{\infty p} >$	T_0	$< q_0 >$	$< q_\infty >$	T_∞	**HPD**
NGC 1199	0.61	0.91	0.093	0.59	0.80	0.34	14.43

NGC 1395	0.73	0.49	0.90	0.66	0.56	0.55	18.43
NGC 1549	0.43	0.91	0.84	0.56	0.74	0.75	4.18

Acknowledgements

We would like to thank the Kalinga University Raipur for the technical support.

References

1. Bak J., Statler T.S., 2000, AJ, 120, 100.
2. Binney J.J., 1985, MNRAS, 212, 767.
3. Chakraborty D.K., 2004, A&A 423, 501
4. Chakraborty D.K., Diwakar A.K., 2011, Astrophysics and Space Sciencs, 331, 419.
5. Chakraborty D.K., Diwakar A.K., Pandey S.K., 2011, MNRAS, 412, 585 (C11).
6. Chakraborty D.K., Singh A.K., Gaffar F., 2008, MNRAS, 383, 1477.
7. Dehnen W., 1993, MNRAS, 265, 250.
8. de Vaucouleurs, 1976, Second Reference Catalogue of Bright Galaxies, University of Texas, Austin, 43.
9. de Zeeuw P.T., Carollo C.M., 1996, MNRAS, 281, 1333.
10. Franx M., Illingworth G., Heckman T. M., 1989, ApJ, 343, 617.
11. Statler T.S., 1994a, ApJ, 425, 458 (S94a).
12. Statler T.S., 1994b, ApJ, 425, 500 (S94b).
13. Statler T. S., 2001, AJ, 121, 244.
14. Statler T.S., Fry A.M.., 1994, ApJ, 425, 481.
15. Statler T.S., Emsellem E., Peletier R.F., Bacon R., 2004, MNRAS, 253, 1.
16. Tenjes P., Busarello G., Lango G., Zaggia S., 1993, A&A, 275, 61.
17. Thakur P., Chakraborty D.K., 2001, MNRAS, 328, 330.